

## THE HUBBLE SPACE TELESCOPE UV LEGACY SURVEY OF GALACTIC GLOBULAR CLUSTERS. VI. THE INTERNAL KINEMATICS OF THE MULTIPLE STELLAR POPULATIONS IN NGC 2808\*

A. BELLINI<sup>1</sup>, E. VESPERINI<sup>2</sup>, G. PIOTTO<sup>3,4</sup>, A. P. MILONE<sup>5</sup>, J. HONG<sup>2</sup>, J. ANDERSON<sup>1</sup>, R. P. VAN DER MAREL<sup>1</sup>, L. R. BEDIN<sup>4</sup>, S. CASSISI<sup>6,7</sup>, F. D'ANTONA<sup>8</sup>, A. F. MARINO<sup>5</sup>, A. RENZINI<sup>4</sup>

*Draft version April 12, 2018*

### Abstract

Numerous observational studies have revealed the ubiquitous presence of multiple stellar populations in globular clusters and cast many hard challenges for the study of the formation and dynamical history of these stellar systems. In this Letter we present the results of a study of the kinematic properties of multiple populations in NGC 2808 based on high-precision *Hubble Space Telescope* proper-motion measurements. In a recent study, Milone et al. have identified five distinct populations (A, B, C, D, and E) in NGC 2808. Populations D and E coincide with the helium-enhanced populations in the middle and the blue main sequences (mMS and bMS) previously discovered by Piotta et al.; populations A, B, and C correspond to the redder main sequence (rMS) that in the Piotta et al. was associated with the primordial stellar population. Our analysis shows that, in the outermost regions probed (between about 1.5 and 2 times the cluster half-light radius), the velocity distribution of populations D and E is radially anisotropic (the deviation from an isotropic distribution is significant at the  $\sim 3.5\text{-}\sigma$  level). Stars of populations D and E have a smaller tangential velocity dispersion than those of populations A, B, and C, while no significant differences are found in the radial-velocity dispersion. We present the results of a numerical simulation showing that the observed differences between the kinematics of these stellar populations are consistent with the expected kinematic fingerprint of the diffusion towards the cluster outer regions of stellar populations initially more centrally concentrated.

*Subject headings:* proper motions — stars: population II — (Galaxy:) globular clusters: individual (NGC 2808) — Galaxy: kinematics and dynamics

### 1. INTRODUCTION

Photometric and spectroscopic studies over the last 15 years have revolutionized our understanding of globular clusters (GCs). Once thought to be “simple stellar populations” with a single age and composition, essentially all GCs host multiple stellar populations (MSPs), as revealed by their multiple photometric sequences. The exquisite precision and stability of the *Hubble Space Telescope* (*HST*) has made much of this possible (see Milone et al. 2015a,b; Nardiello et al. 2015; Piotta et al. 2015, and references therein). MSPs can be traced to different compositions in terms of light elements (such as Na, O, Al, Mg observed spectroscopically; see Gratton et al. 2012 and references therein) and He Pasquini et al. 2011; Villanova et al. 2012; Marino et al. 2014). These observational findings have cast a number of challenges for the study of the formation and evolution of

GCs.

In order to make progress toward a complete picture of the formation and evolutionary history of GCs, as well as to constrain the possible paths for the theoretical study of these complex challenges and questions, a major effort to combine observational data is essential. Spectroscopic and photometric studies have begun to shed light on the chemical properties, number of distinct sequences and range of ages of different stellar populations.

Structural and kinematic properties of different stellar populations are two additional key pieces of the puzzle, as they contain essential information to build a complete picture of MSP cluster formation and dynamical evolution. According to a number of different formation scenarios (see, e.g., D’Ercole et al. 2008; Decressin et al. 2007; Bastian et al. 2013), second-generation (2G) populations should form more concentrated in the cluster inner regions<sup>1</sup> Numerical simulations (Vesperini et al. 2013) have shown that several clusters should still retain some memory of this initial spatial segregation and a few observational studies have indeed found clusters in which 2G stars are still concentrated in the cluster inner regions (Sollima et al. 2007; Bellini et al. 2009a; Johnson & Pilachowski 2012; Milone et al. 2012; Lardo et al. 2011; Bellini et al. 2013a; Cordero et al. 2014).

Little is however known to-date on the proper-motion (PM) based kinematics of MSPs (with the only exceptions of  $\omega$  Cen and 47 Tuc: Bellini et al. 2009b; Anderson & van der Marel 2010; Richer et al. 2013). Richer et al. (2013) probed the outer regions of 47 Tuc (at  $\sim 1.9 r_h$ ) and found that 2G stars are characterized by a radially anisotropic velocity distribution while the 1G population is isotropic. As discussed in Section 4, this trend is consistent with the expected kinematical

\* Based on observations with the NASA/ESA *Hubble Space Telescope*, obtained at the Space Telescope Science Institute, which is operated by AURA, Inc., under NASA contract NAS 5-26555.

<sup>1</sup> Space Telescope Science Institute, 3700 San Martin Dr., Baltimore, MD 21218, USA

<sup>2</sup> Department of Astronomy, Indiana University, Bloomington, IN 47405, USA

<sup>3</sup> Dipartimento di Fisica e Astronomia “Galileo Galilei”, Università di Padova, v.co dell’Osservatorio 3, I-35122, Padova, Italy

<sup>4</sup> Istituto Nazionale di Astrofisica, Osservatorio Astronomico di Padova, v.co dell’Osservatorio 5, I-35122, Padova, Italy

<sup>5</sup> Research School of Astronomy & Astrophysics, Australian National University, Mt Stromlo Observatory, via Cotter Rd, Weston, ACT 2611, Australia

<sup>6</sup> Istituto Nazionale di Astrofisica, Osservatorio Astronomico di Teramo, Via Mentore Maggini s.n.c., I-64100, Teramo, Italy

<sup>7</sup> Instituto de Astrofísica de Canarias, E-38200 La Laguna, Tenerife, Canary Islands, Spain

<sup>8</sup> Istituto Nazionale di Astrofisica, Osservatorio Astronomico di Roma, Via Frascati 33, I-00040, Monteporzio Catone, Roma, Italy

<sup>1</sup> Hereafter, we will use “populations” and “generations” as synonyms.

implications of the formation models mentioned above; the study presented in this Letter is aimed at exploring whether the kinematics of MSPs in NGC 2808 further confirms this general expectation and the trend identified in 47 Tuc.

NGC 2808 is one of the most massive Galactic GCs and one of the most massive Galactic GCs and one of the few known to host a super-He-rich subpopulation (see, e.g., D’Antona et al. 2005; Piotto et al. 2007). The initial picture of three distinct stellar populations found by Piotto et al. (2007) has been recently shown to be even more complex by Milone et al. (2015b), who identified five distinct populations (named A, B, C, D and E) along the red-giant branch (RGB) and the main sequence (MS) of NGC 2808. We point out here that populations D and E correspond to the 2G populations identified by Piotto et al. (2007, their mMS and bMS). Populations A, B, and C correspond to the rMS of the Piotto et al. (2007) study (that they assumed to be the first generation, 1G). New WFC3/UVIS UV data (GO-12605, PI: Piotto) allowed us to further split the rMS into the three populations A, B and C. Available spectroscopic data discussed in Milone et al. (2015b) suggest that population B has Na and O abundances usually associated with 1G stars; population C includes stars with slightly enhanced Na and slightly depleted O abundances, and is photometrically distinct from population B along the RGB (see Milone et al. 2015b, their Fig. 8). No spectroscopic data are available to further characterize population A.

In this Letter we shed further light on the properties of this complex cluster and present an analysis of the internal PMs of its five stellar populations. The outline of this Letter is as follows: in Section 2 we describe the data sets and reduction; in Section 3 we present our results on the kinematic properties of the five populations identified in NGC 2808. In Section 4 we discuss the interpretation of the observational findings. We summarize our conclusions in Section 5.

## 2. DATA SETS AND REDUCTION

We have compiled high-precision PM catalogs for the central regions of 22 GCs, mostly based on the archival *HST* proposal AR-12845 (P.I.: Bellini, see Bellini et al. 2014). PMs are obtained following the *central overlap* method (Eichhorn & Jefferys 1971), via a careful data-rejection process. Extensive simulations have demonstrated the reliability of the estimated PMs and their errors. The observations used to compute PMs in NGC 2808 are listed in Table 11 of Bellini et al. (2014). We additionally included WFC3/UVIS observations of GO-12605 ( $6 \times 650$  s in F336W and  $6 \times 97$  s in F438W), taken in 2013, to further extend the available time baseline and increase the PM accuracy. The catalog contains over 86000 stars down to  $\sim 5$  mag below the turn off (TO). Well-measured stars have a typical PM error of less than  $\sim 30 \mu\text{as yr}^{-1}$  ( $\sim 1.3 \text{ km s}^{-1}$ , at a distance of 9.6 kpc, Harris 1996).

The photometric catalog of Milone et al. (2015b) combines the GO-10775 F606W and F814W ACS/WFC photometry presented in Anderson et al. (2008) with the WFC3/UVIS F275W, F336W and F438W exposures of GO-12605. All observations were corrected for CTE effects (Anderson & Bedin 2010) and reduced using the software family *img2xym* (Anderson et al. 2006), employing spatially-varying, time-dependent empirical PSFs (Bellini et al. 2013b). Stellar positions were corrected for geometric distortion following the recipes in Bellini & Bedin (2009) and Bellini, Anderson & Bedin (2011). Photometry is

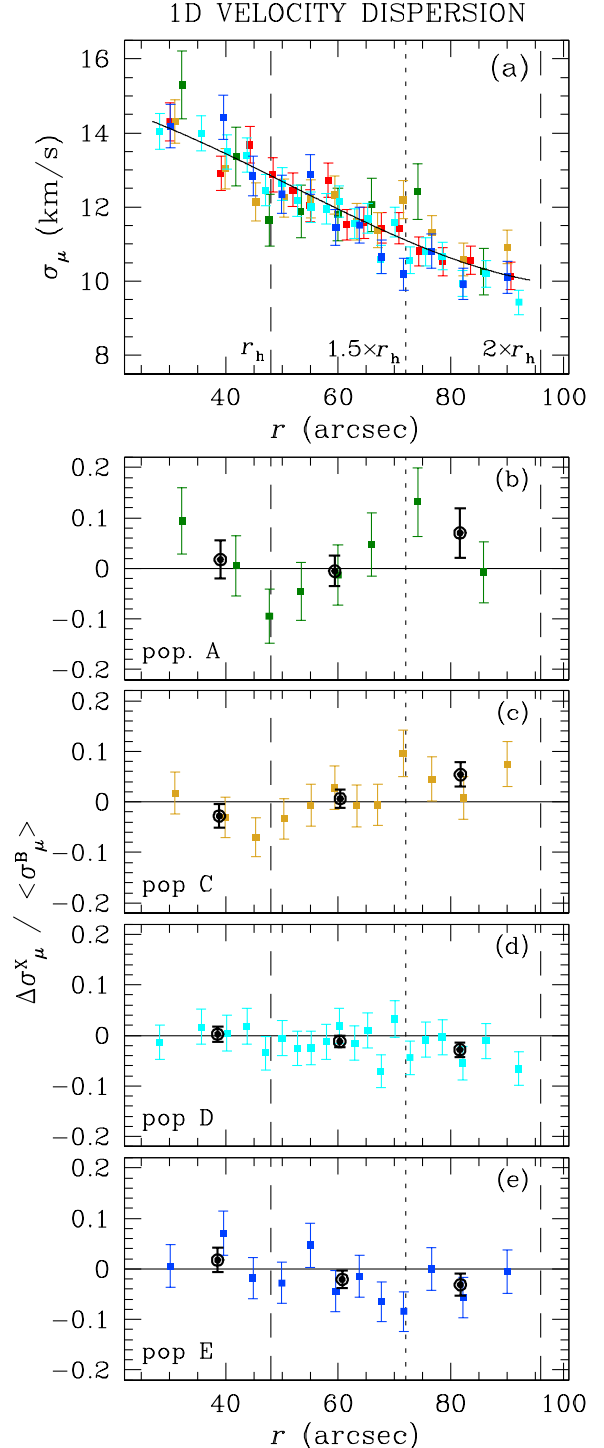


**Figure 1.** (a) 1D  $\sigma_\mu$  vs.  $r$  for the 5 distinct populations. We least-squares fitted a 3rd-order polynomial to the population B profile ( $\langle\sigma_\mu^B\rangle$ ) (black curve). The half light radius,  $1.5 \times r_h$ , and  $2 \times r_h$  (dashed and dotted lines) are also indicated. Panels (b) to (e) show the normalized difference between  $\sigma_\mu$  of populations A, C, D, E, respectively, with respect to that of the reference population B. Colored points refer to bins containing the same number of stars per population. Black points refer to 3 fixed radial intervals: (1)  $r \leq r_h$ , (2)  $r_h < r \leq 1.5 \times r_h$ , and (3)  $1.5 \times r_h < r \leq 2 \times r_h$ . See the text for details.

calibrated as in Bedin et al. (2005).

We refer to Bellini et al. (2014) and Milone et al. (2015b) for a detailed description of the data reduction.

The cross-identification of common stars between the PM

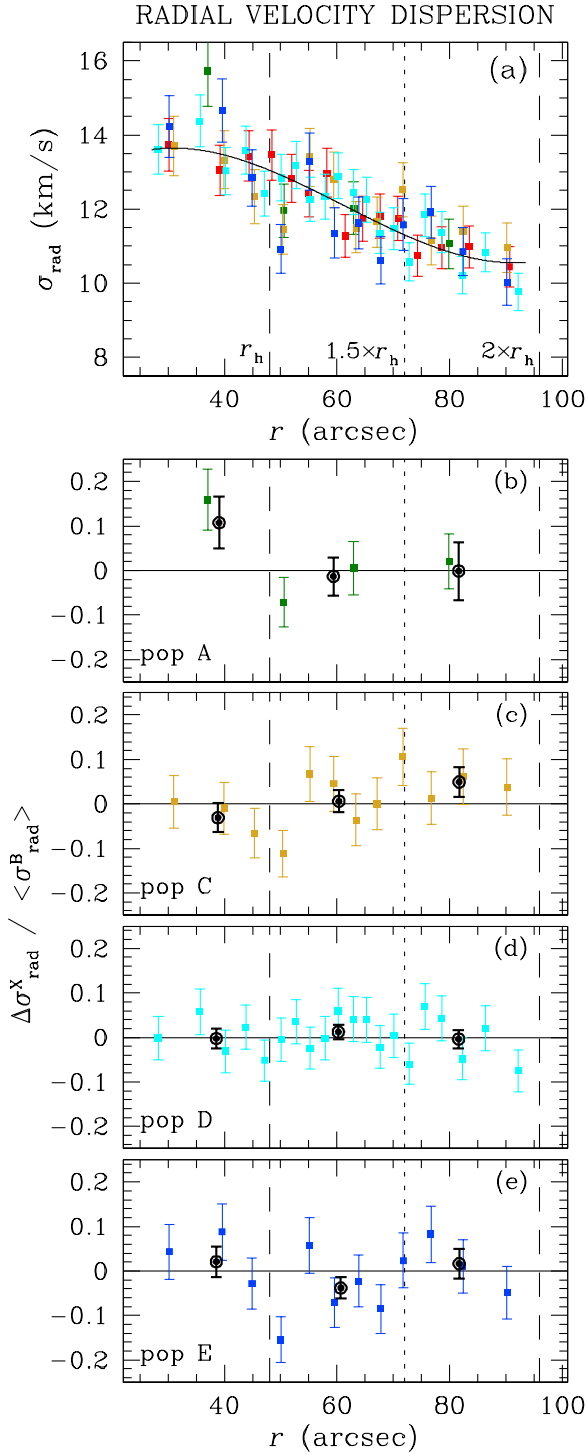


**Figure 2.** Similar to Fig. 1 but for the radial component of the motion. See the text for details.

and the photometric catalog left us with near 38000 objects down to about 3 mag below the TO. In order to analyze in detail the internal kinematics of NGC 2808 stars, particular care must be taken in removing any PM measurements affected by systematic effects. To this aim, we closely followed the recipes described in detail in Section 7.5 of Bellini et al. (2014). Our final sample consists of about 27000 stars within  $115''$  (the outermost corner of the field of view) with high-precision, high-quality measurements.

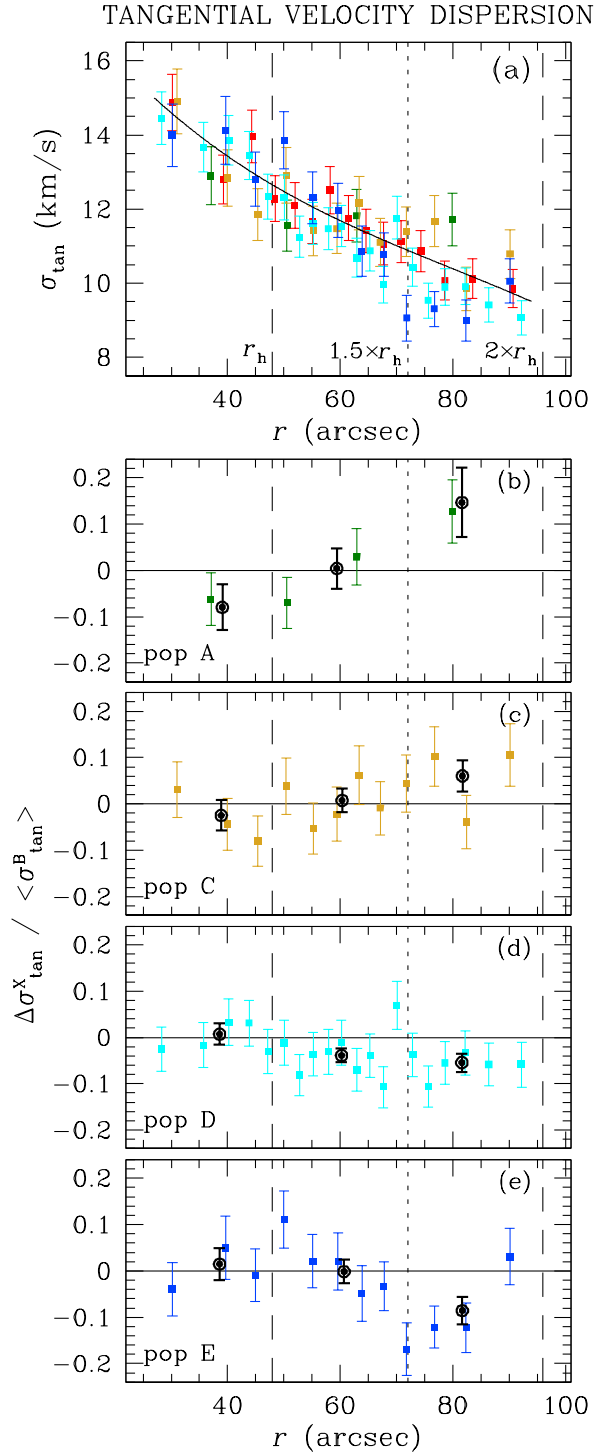


**Figure 3.** Similar to Fig. 1 but for the tangential component of the motion. See the text for details.

### 3. THE INTERNAL KINEMATICS OF THE FIVE SUBPOPULATIONS

To avoid edge effects, we consider hereafter only stars within  $2 \times r_h = 96''$  (Harris 1996, 2010 edition). Due to small-number statistics, the kinematics of the MSPs on the RGB cannot be studied with sufficient detail. On the other hand, we have plenty of MS stars at our disposal, in particular: 598 population-A stars, 3071 B, 1875 C, 4485 D, and 1814 E. We will use the same nomenclature and color-coding of Milone et al. (2015b).

The 1D average transverse velocity-dispersion profile  $\sigma_\mu$  of each population, obtained by combining together  $\mu_\alpha \cos \delta$  and  $\mu_\delta$ , is shown in panel (a) of Fig. 1. We binned each population in such a way as to have the same number of measurements ( $\gtrsim 150$ ) in each bin. We marked the position of  $r_h$  (inner dashed line),  $1.5 \times r_h$  (dotted line), and  $2 \times r_h$  (outer dashed line). All errorbars refer to  $1\text{-}\sigma$  errors.

The five profiles largely follow the same trend. To better examine small velocity-dispersion differences among them we proceeded as follows. We chose population B (He-normal, 1G stars) as a reference, and we least-squares fitted a 3rd-order polynomial to its  $\sigma_\mu$  profile (red points in panel a) to obtain the average trend  $\langle \sigma_\mu^B \rangle$ . Then, we computed the differences  $\Delta\sigma_\mu^X$  between the  $\sigma_\mu$  of the other 4 populations ( $X = A, C, D, E$ ) and the average trend of population B at the same radial distance. These quantities are then normalized to the average trend of population B itself. These normalized differences are shown in panels (b) to (e), as a function of  $r$ , for populations A, C, D and E, respectively.

In addition, we binned each population into 3 radial intervals: (1)  $r \leq r_h$ , (2)  $r_h < r \leq 1.5 \times r_h$ , and (3)  $1.5 \times r_h < r \leq 2 \times r_h$ . The respective values of  $\Delta\sigma_\mu^X / \langle \sigma_\mu^B \rangle$  for these radial bins are shown as black points with errorbars. Populations A and C (panels b and c) exhibit a slightly increasing  $\Delta\sigma_\mu^X / \langle \sigma_\mu^B \rangle$  values the larger the radial distance, while populations D and E (panels d and e) seem to have an opposite behavior. These differences are marginally significant (at the  $2\text{-}\sigma$  level).

We repeated the same analysis shown in Fig. 1 independently for the radial and tangential components of motion.<sup>2</sup> Results are shown in Fig. 2 and 3 for the radial ( $\sigma_{\text{rad}}$ ) and tangential ( $\sigma_{\text{tan}}$ ) velocity-dispersion profiles, respectively.

First, we note the overall trend of  $\sigma_{\text{tan}}$  (Fig. 3a) being smaller than  $\sigma_{\text{rad}}$  (Fig. 2a) for  $r \gtrsim r_h$ , in agreement with what found by Watkins et al. (2015) for the RGB of this cluster. The *radial* velocity dispersions of the 5 populations do not show significant differences (with only possible hints, at less than  $\sim 2\text{-}\sigma$  level, of a larger  $\sigma_{\text{rad}}$  of population A in the innermost region, a larger  $\sigma_{\text{rad}}$  for population C in the outermost bin), while for  $r > 1.5 \times r_h$  the *tangential* velocity dispersion of populations D and E (panels d and e of Fig. 3) is significantly smaller ( $-0.054 \pm 0.019$  for D, and  $-0.086 \pm 0.028$  for E, i.e., at the  $2.8\text{-}$  and  $3.1\text{-}\sigma$  level, respectively) than that of the reference population B. No significant difference is instead found between the kinematics of population B and that of A and C, with only a hint (at less than  $\sim 2\text{-}\sigma$  level) of a larger tangential velocity for populations A and C in the outermost regions (panels b and c of Fig 3)

To further explore these findings, we computed the radial dependence of the deviation from isotropy ( $\sigma_{\text{tan}}/\sigma_{\text{rad}} - 1$ ) of each population. Results are shown in Fig. 4. The horizontal line at 0 corresponds to an isotropic system. As for Fig. 1, larger black dots refer to data binned in the 3 radial intervals, while colored points are used for data binned by keeping the same number of stars per bin.

Populations B and C have an overall similar trend, and tend to very slightly deviate from isotropy outside  $r_h$ . In the outermost regions probed (between  $1.5r_h$ , and  $2r_h$ ) populations D and E are radially anisotropic ( $\sigma_{\text{tan}}/\sigma_{\text{rad}} - 1$  equal to  $-0.093 \pm 0.027$  for D and  $-0.140 \pm 0.040$  for E: a deviation from an isotropic distribution at the  $\sim 3.4\text{-}\sigma$  and  $3.5\text{-}\sigma$  level,

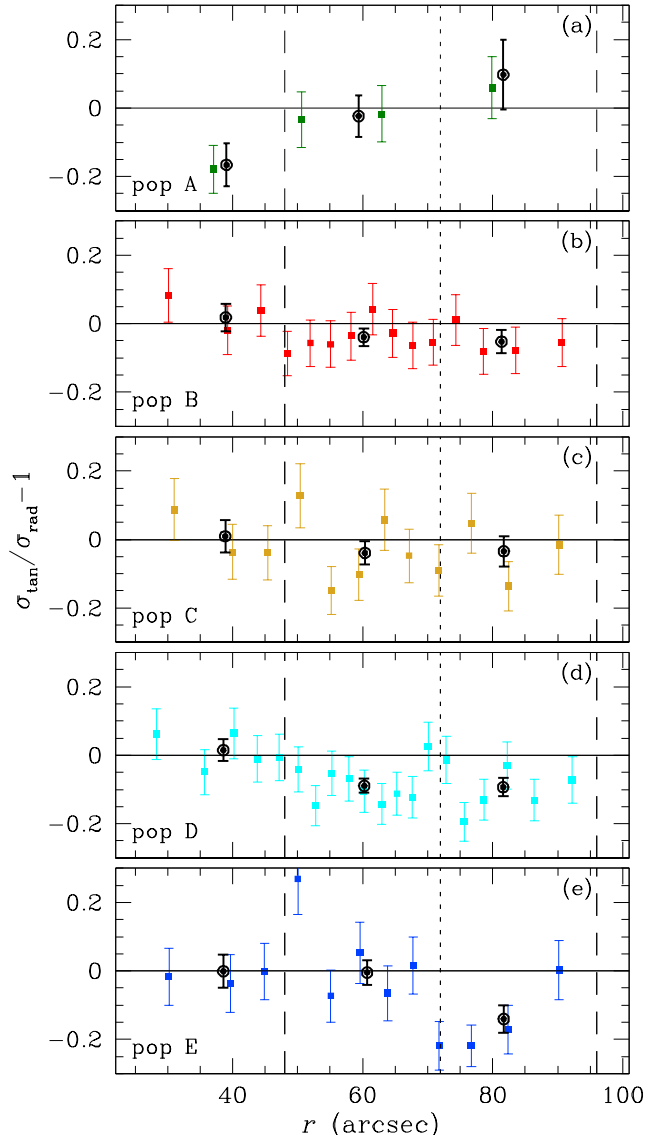


**Figure 4.** Deviation from tangential-to-radial isotropy (horizontal line) for the 5 populations (color-coded as in Fig. 1). Vertical lines mark the locations of  $r_h$ ,  $1.5 \times r_h$ , and  $2 \times r_h$ .

respectively). There is a hint of population A having an opposite behavior with respect to the others: the outer 2 points are fairly consistent with an isotropic system, while the innermost point indicates a marginally-significant (at the  $\sim 2\text{-}\sigma$  level) radial anisotropy for  $r < r_h$ . As discussed in the Introduction, the nature of population A is still unclear and spectroscopic data will be necessary to characterize this population in the context of the MSPs of NGC 2808. Additional kinematic data would also be necessary to shed further light on the kinematic properties of this population and clarify the significance of possible kinematic anomalies.

#### 4. THEORETICAL INTERPRETATION

The two most statistically-significant results presented in the previous sections are: i) populations D and E have a radially anisotropic velocity distribution (Fig. 4) in the outermost regions, and ii) this difference in anisotropy is due to the fact that populations D and E have a smaller tangential velocity dispersion than that of the other populations (Fig. 3). No strong differences are instead found in the radial velocity

<sup>2</sup> We decreased the number of bins while keeping the same number of measurements within (at least 150) for populations A, D and E.

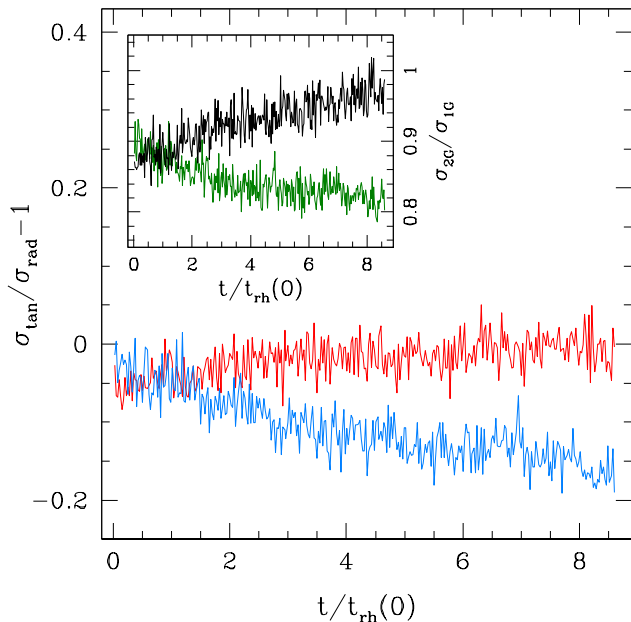


**Figure 5.** Time evolution of  $\sigma_{\text{tan}}/\sigma_{\text{rad}} - 1$  measured for particles between  $1.5$  and  $2 r_h$  for the 2G (blue line) and the 1G (red line) populations (where  $r_h$  is the projected half-mass radius). The green line in the inset shows the time evolution of the mean of the ratio of the 2G to the 1G tangential velocity dispersion, while the black line is for the mean of the ratio of the 2G to the 1G radial velocity dispersion (both measured between  $1.5$  and  $2 r_h$ ). Time is normalized to the initial half-mass relaxation time (calculated using the projected half-mass radius).

dispersion of all the populations (see Fig. 2).

One of the predictions of MSP cluster-formation models, in which asymptotic-giant branch (AGB) stars are the source of gas out of which 2G stars form, is that the AGB ejecta would collect in the cluster central regions and 2G stars would initially be more spatially concentrated than the 1G population (D’Ercole et al. 2008). Other formation models, based on rapidly-rotating massive stars and/or massive binaries (see e.g. Decressin et al. 2007; de Mink et al. 2009; Bastian et al. 2013) do not follow the evolution of the processed gas but assume that massive stars are initially concentrated in the cluster inner regions and so is the gas they release. In any case, the subsequent long-term dynamical evolution will gradually erase the differences in the spatial distribution of 1G and 2G stars.

Here, we present the results of a N-body simulation carried out to explore the evolution of the kinematical properties of different stellar populations. We started our simulation with 50000 equal-mass particles, with 1G and 2G populations having the same total mass and both following a King (1966) model density profile with central dimensionless potential  $W_0 = 7$ . We assumed that the 2G population is more centrally concentrated, with an initial half-mass radius about 4.5 times smaller than that of the 1G population. As for the kinematical properties, both 1G and 2G systems are initially isotropic. The cluster is initially tidally limited and is assumed to move on a circular orbit in the external potential of the host galaxy (modeled as a point mass). We point out that we are not ruling out the possibility that the formation process and the subsequent virialization phase might result in 1G and 2G subsystems with initially different anisotropy profiles, but here we focus solely on the role of relaxation-driven long-term dynamical evolution in establishing kinematical differences between different stellar populations. This

simulation has been run with the GPU-accelerated version of the NBODY6 code (Aarseth 2003; Nitadori & Aarseth 2012) on the Big Red II supercomputer at Indiana University.

Observational data reveal that the strongest deviation from isotropy occurs in the outermost regions for which data are available. Figure 5 shows the time evolution of  $\sigma_{\text{tan}}/\sigma_{\text{rad}} - 1$  measured for particles between  $1.5$  and  $2 r_h$  (where  $r_h$  is the projected half-mass radius) for the 2G and the 1G populations, where  $\sigma_{\text{rad}}$  and  $\sigma_{\text{tan}}$  are, respectively, the projected radial and tangential velocity dispersions as measured on a plane coinciding with the cluster orbital plane. This is the outermost region probed by our observational data where the difference in anisotropy between 1G and 2G populations is strongest. The results of our simulation show a trend qualitatively consistent with that found in the observational data: as 2G stars diffuse from the inner regions (where they formed and are initially segregated), they populate the outer cluster regions preferentially on radial orbits as shown by the increasing radial anisotropy of the 2G population. The trend found in our simulation agrees with what was found in a recent numerical study by Henault-Brunet et al. (2015). The different formation and dynamical history of 1G and 2G stars, which are currently located in the same outer region of the cluster (in this case between  $1.5$  and  $2 r_h$ ), is revealed by the differences in the kinematic properties. These differences are stronger in the cluster’s outer regions, which are initially dominated by 1G stars. As the cluster evolves, the cluster’s outer regions are populated also by 2G stars, diffused from their initial inner location.

The inset of Fig. 5 shows the time evolution of the mean of the ratio of the 1G to the 2G  $\sigma_{\text{rad}}$  and  $\sigma_{\text{tan}}$ , measured between  $1.5$  and  $2 r_h$ . The initial differences in the  $\sigma_{\text{rad}}$  and  $\sigma_{\text{tan}}$  of the two populations evolve in a direction consistent with the observed trends: the radial velocity dispersion  $\sigma_{\text{rad}}$  of the two populations becomes increasingly similar while  $\sigma_{\text{tan}}$  of the 2G becomes smaller than that of the 1G and, in agreement with our observational findings. It is this difference that is responsible for the differences in the anisotropy of the two populations.

## 5. CONCLUSIONS

In this Letter we have presented an *HST* study of the kinematical properties of the MSPs of NGC 2808 based on high-precision PM measurements (Bellini et al. 2014). In a recent study, Milone et al. (2015b) identified five different populations in this cluster: two of these populations (named D and E) correspond to the 2G populations in the mMS and bMS identified in an earlier study by Piotto et al. (2007) while the other three populations (A, B, and C) correspond to the rMS population in the Piotto et al.’s study. In this Letter we show that the five stellar populations of this cluster are characterized by differences in their kinematics.

Specifically, we find that in the outermost regions probed (between  $1.5$  and  $2 r_h$ ) the velocity distribution of the 2G populations D and E is radially anisotropic (the deviation from isotropy being significant at the  $\sim 3.5\text{-}\sigma$  level). Our data show that the larger radial anisotropy in the 2G populations D and E is due to the fact that these populations have smaller tangential velocity dispersions than the other populations. Qualitatively similar trends have been found by Richer et al. 2013 in 47 Tuc. No significant differences are found in the radial velocity dispersions of all the populations and between the kinematics of population B and that of A and C (with only possible hints of a larger  $\sigma_{\text{rad}}$  of population A in the inner-

most region, a larger  $\sigma_{\text{rad}}$  for population C in the outermost bin, and a larger  $\sigma_{\text{tan}}$  for populations A and C in the outermost regions all at less than  $2\text{-}\sigma$  level).

The results of an N-body simulation show that the differences in both the radial anisotropy and in the tangential velocity dispersion observed for populations D and E are consistent with being the kinematical fingerprint of the diffusion of 2G populations from the innermost regions, where they are initially concentrated, towards the cluster outer regions. A more extended survey of models, probing broader ranges of different initial conditions, is necessary to fully explore the possible evolutionary paths of the 1G and 2G kinematical properties and their dependence on initial conditions.

On the observational side, we emphasize the importance of extending the current study to even more external cluster regions. In fact, the outermost regions are essential for a complete characterization of a cluster's kinematical properties and, in particular, to shed light on the possible effects of the external Galactic tidal field. These effects are expected to limit the outer development of the radial anisotropy and make these more isotropic (and possibly even slightly tangentially anisotropic).

We plan to extend the analysis presented here to other GCs as possible, using the PM catalogs of Bellini et al. (2014) in combination with the UV photometry of Piotto et al. (2015). This will create a substantial case history that will help us in better understanding formation and evolution of MSPs in GCs.

Support for this work comes from STScI grants for HST programs AR-12845 and GO-13297. E.V. acknowledges support also by grant NASA-NNX13AF45G. G.P., S.C., F.D'A. and A.R. acknowledge support from PRIN-INAF 2014 (PI: S. Cassisi).

#### REFERENCES

- Aarseth, S. J. 2003, *Gravitational N-Body Simulations*, by Sverre J. Aarseth, pp. 430. ISBN 0521432723. Cambridge, UK: Cambridge University Press, November 2003
- Anderson, J., & King, I. R. 2006, *ACS/ISR 2006-01* (Baltimore, MD: STScI), available online at <http://www.stsci.edu/hst/acs/documents/isrs>
- Anderson, J., Sarajedini, A., Bedin, L. R., et al. 2008, *AJ*, 135, 2055
- Anderson, J., & van der Marel, R. P. 2010, *ApJ*, 710, 1032
- Anderson, J., & Bedin, L. R. 2010, *PASP*, 122, 1035
- Bastian N. et al. 2013, *MNRAS*, 436, 2398
- Bedin, L. R., Cassisi, S., Castelli, F., et al. 2005, *MNRAS*, 357, 1038
- Bellini, A., Piotto, G., Bedin, L. R., et al. 2009a, *A&A*, 507, 1393
- Bellini, A., Piotto, G., Bedin, L. R., et al. 2009b, *A&A*, 493, 959
- Bellini, A., & Bedin, L. R. 2009, *PASP*, 121, 1419
- Bellini, A., Anderson, J., & Bedin, L. R. 2011, *PASP*, 123, 622
- Bellini, A., Piotto, G., Milone, A. P., et al. 2013, *ApJ*, 765, 32
- Bellini, A., Anderson, J., Salaris, M., et al. 2013, *ApJ*, 769, L32
- Bellini, A., Anderson, J., van der Marel, R. P., et al. 2014, *ApJ*, 797, 115
- Carretta, E. 2014, *ApJ*, 795, L28
- Cordero, M. J.; Pilachowski, C. A.; Johnson, C. I.; McDonald, I.; Zijlstra, A. A.; Simmerer, J., 2014, *ApJ*, 780, 94
- D'Antona, F., Bellazzini, M., Caloi, V., et al. 2005, *ApJ*, 631, 868
- D'Ercole A., Vesperini E., D'Antona F., McMillan, S.L.W., Recchi, S., 2008, *MNRAS*, 391, 825
- de Mink, S. E., Pols, O. R., Langer, N., & Izzard, R. G. 2009, *A&A*, 507, L1
- Decressin, T., Meynet, G., Charbonnel C. Prantzos, N., Ekstrom, S. 2007, *Å*, 464, 1029
- Eichhorn, H., & Jefferys, W. H. 1971, *Publications of the Leander McCormick Observatory*, 16, 267
- Gratton, R. G., Carretta, E., & Bragaglia, A. 2012, *A&A Rev.*, 20, 50
- Harris, W.E. 1996, *AJ*, 112, 1487 (2010 edition)
- Henault-Brunet, V., Gieles, M., Agertz, O., Read, J. I., 2015, *MNRAS*, 450, 1164
- Johnson C. I., Pilachowski C. A., 2012, *ApJ*, 754, L38
- King, I. R. 1966, *AJ*, 71, 64
- Lardo, C., Bellazzini, M., Pancino, E., et al. 2011, *A&A*, 525, A114
- Marino, A. F., Milone, A. P., Przybilla, N., et al. 2014, *MNRAS*, 437, 1609
- Milone, A. P., Piotto, G., Bedin, L. R., et al. 2012, *A&A*, 537, AA77
- Milone, A. P., Marino, A. F., Piotto, G., et al. 2015a, *MNRAS*, 447, 927
- Milone, A. P., Marino, A. F., Piotto, G., et al. 2015, *ApJ*, 808, 51
- Nardiello, D., Piotto, G., Milone, A. P., et al. 2015, *arXiv:1504.07876*
- Nitadori, K., & Aarseth, S. J. 2012, *MNRAS*, 424, 545
- Pasquini, L., Mauas, P., Käufel, H. U., & Cacciari, C. 2011, *A&A*, 531, A35
- Pietrinferni, A., Cassisi, S., Salaris, M., & Castelli, F. 2004, *ApJ*, 612, 168
- Pietrinferni, A., Cassisi, S., Salaris, M., Percival, S., & Ferguson, J. W. 2009, *ApJ*, 697, 275
- Piotto, G., Bedin, L. R., Anderson, J., et al. 2007, *ApJ*, 661, L53
- Piotto, G., Milone, A. P., Bedin, L. R., et al. 2015, *AJ*, 149, 91
- Richer, H. B., Heyl, J., Anderson, J., et al. 2013, *ApJ*, 771, L15
- Sollima, A., Ferraro, F. R., Bellazzini, M., et al. 2007, *ApJ*, 654, 915
- Vesperini, E.; McMillan, S. L. W.; D'Antona, F.; D'Ercole, A., 2013, *MNRAS*, 429, 1913
- Villanova, S., Geisler, D., Piotto, G., & Gratton, R. G. 2012, *ApJ*, 748, 62
- Watkins, L. L., van der Marel, R. P., Bellini, A., & Anderson, J. 2015, *ApJ*, 803, 29